



Non-isothermal crystallization kinetics of polyethylene terephthalate: a study based on Tobin, Hay and Nakamura models

Abdollah Sheikh Nezhad Moghadam¹ · Mehdi Rafizadeh^{1,2} · Faramarz Afshar Taromi^{1,2}

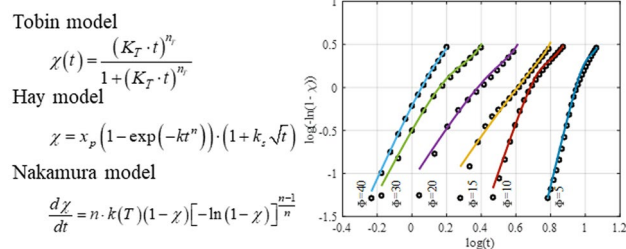
Received: 1 July 2022 / Accepted: 11 September 2022 / Published online: 25 October 2022
© Iran Polymer and Petrochemical Institute 2022

Abstract

Appropriate knowledge of non-isothermal crystallization kinetics of polyethylene terephthalate is vital in producing final polymeric parts with a certain degree of crystallization. Hence, PET was synthesized through a two-step esterification and polycondensation method. The structure of prepared PET was examined using FTIR and NMR tests. Due to the practical applications of the crystallization process, non-isothermal crystallization of PET was studied from the melt state under various cooling rates (Φ) between 5 and 40 K/min using DSC, demonstrating a wide range of Φ . The experimental results revealed that the crystallization reaches its final value for the cooling rates of 5 and 10 K/min. However, a partial crystallization occurred under higher cooling rates. The recrystallization of these samples during heating was confirmed. Empirical data showed no meaningful change in T_g and T_m with cooling rate. However, T_C and the final degree of crystallization varied linearly with cooling rate. Crystallization kinetic models are classified into two types: nonlinear and those that can be converted to linear. Due to the secondary crystallization of PET, the Avrami model could not make a good prediction. Among the linearizable models, Tobin model fitted the results very well. Among the nonlinear forms, the recently developed Hay model has an excellent ability to describe non-isothermal kinetics. Moreover, the integral type of Nakamura model was fitted instead of the normal differentiation form. A two-step optimization method is presented to achieve a high regression coefficient for nonlinear fitted models.

Graphical Abstract

Evaluating Various Models of Non-Isothermal Crystallization Kinetics of Polyethylene Terephthalate from Melt State under Various Cooling Rates



Keywords Polyethylene terephthalate · Non-isothermal · Crystallization kinetics · Tobin model · Hay model · Nakamura model

✉ Mehdi Rafizadeh
mehdi@aut.ac.ir

¹ Polymer Engineering Department, Amirkabir University of Technology of Mahshahr Campus, Bandar Mahshahr, Khuzestan, Iran

² Department of Polymer Engineering and Color Technology, Amirkabir University of Technology, Tehran, Iran

Introduction

Polyethylene terephthalate (PET) is the most important commercial member of thermoplastic polyesters produced globally. The final properties of PET parts are related to

its microstructure, which is formed during the production process or its cycle life. Amorphous and semi-crystalline are the two main types of microstructures that are constructed based on thermomechanical history. Differential scanning calorimetry (DSC) is the most widely used in crystallization studies. In the cooling and heating curves, amorphous polymers show the glass transition temperature (T_g), which is the change from the glassy state to the melt phase. Apart from T_g , semi-crystalline polymers also exhibit additional transitions, such as crystallization and melting [1]. Reorganization of polymer morphology, structure and chain conformation can affect the crystallization kinetics and final properties [2]. Recently, a three-phase model for thermoplastic polyesters, especially PET, has been presented. It was concluded that PET consists of a large fraction of rigid amorphous region [3]. Manipulating crystallization variables makes it possible to reach a great variety of microstructures. PET morphology and its effect on properties have been studied by many researchers. Jog [4] presented an outstanding review on the crystallization of PET. Controlling the crystallization process can affect the orientation and crystallite perfection. Therefore, properties of the final products could be found by acquiring deeper insight into the crystallization process [4]. Pressure, molecular weight, catalyst and production conditions affect the crystallization behavior of PET in either isothermal or non-isothermal processes [5–8]. Crystallization rate, morphology, and other characteristics could be manipulated by adding a nucleating agent. Up to the present various nucleating agents, such as talc, sodium benzoate, ionomer Na^+ , calcium carbonate and cassava starch have been reported [9–11]. Even sodium salts, such as $-\text{CO}_2\text{Na}$, $-\text{ONa}$, SO_3Na and $-\text{PO}_3\text{Na}$, as nucleating agent, have been added to PET through the in situ polymerization and crystallization of PET [12]. Chemical structure manipulation, such as copolymerization, branching and compounding, are among interesting methods to change crystallization behavior [13–15]. The crystallization behavior and mechanical properties of PET and polylactic acid (PLA) blends were investigated during an in-depth study [16]. Different techniques have been employed to study the crystallization kinetics, in which measurement of density is applicable [17]; X-ray diffraction has been applied to determine the degree of crystallinity of PET-oriented films and fibers [18–20]; terahertz time-domain spectroscopy (THz-TDS) has been harnessed to monitor the isothermal crystallization kinetics of amorphous PET [21]; Raman spectroscopy has been utilized to study the kinetics of an initially quasi-amorphous PET [1]. DSC is among the most effective thermal analysis methods for studying the structure and properties of polymers [2, 22]. Moreover, knowledge of crystallization could have a variety of industrial applications, such as preparing PET granules upon solid-state polymerization (SSP) to reach higher molecular weights [23]. Moreover, polymers have

been used as a nucleating agent in crystallization processes [24]. It is well known that PET has a secondary crystallization phenomenon [25]; hence, the overall crystallization consists of primary and secondary ones [26]. Primary and secondary crystallization processes occur simultaneously, affecting kinetics parameters [27]. Crystallization kinetics of isothermal and non-isothermal mathematical modeling are under investigation. Providing mathematical models for crystallization kinetics, isothermal or non-isothermal, is a valuable tool for applying the required microstructure of semi-crystalline polymers. Many Models have been introduced, such as Avrami, Ozawa, Ziabicki, Tobin, Hay, Nakamura, etc. [28, 29]. The Avrami model has been the most reported model for various polymers [30–32]. A review of the literature shows that the crystallization kinetics of polymers, such as PET, has been under intensive investigation. However, ongoing research and recent achievements in this field make it necessary to apply these results to PET. The use of new models, such as the Hay model, has not been reported. Moreover, most of the reported data are within a small range of cooling rates. The crystallization behavior of commercially available PET can be affected by the additives present. Studies on neat PET can help to estimate additive effects. In this work, PET was synthesized through two-step esterification and polycondensation method, and PET samples with no additives and fillers were obtained. Upon characterization of the PET samples, using FTIR and NMR, non-isothermal crystallization was studied using DSC under a wide range of cooling rates, namely, 5, 10, 15, 20, 30 and 40 K/min from a melt state. Different kinetics models were applied by evaluating their related parameters. Due to the convergence problem in model fitting, an algorithm was depicted to reach the regression coefficient as close as possible to 1.0000. Such results can be used in processing of polymers to have final products with various applications. Moreover, this is the first time that Tobin, Hat and Nakamura's models are applied to PET over such a wide range of cooling rates.

Experimental

Materials

The primary reactants used are ethylene glycol (EG) and terephthalic acid (TPA), which were supplied by Shahid Tondgooyan Petrochemical Company (STPC). Antimony oxide, as the polycondensation catalyst, was prepared by Polychem Industrial Co., Ltd., China. Dichloroacetic acid as a solvent in measuring intrinsic viscosity, *ortho*-cresol and chloroform as solvents in measuring the acid end group, and potassium hydroxide as a potentiometry agent were bought from Merck Co., Germany.

Synthesis of polyethylene terephthalate

All samples were prepared in a home-made laboratory-scale reactor. This setup consists of a one-liter stainless steel reactor, EG condenser, water separator, heating system, and vacuum pump as the main constituents of the system. Some preliminary runs were performed to determine the suitable synthesis condition to obtain a polymer with adequate intrinsic viscosity and molecular weight. In each run, 248.70 g of EG and 475.5 g of TPA were agitated for 20 min in laboratory conditions before pouring into the reactor. Next, the reactor was completely sealed. During the esterification step, the EG condenser temperature was 433 K. The inner reactor temperature was controlled above 468 K, around 2 bar pressure and agitated for 15 min. Next, the mixture temperature and pressure were elevated to 528 K and 5 bar, respectively. Water production is an indication of esterification reaction. The condensed water was collected every 15 min to determine the reaction progress. The esterification step terminates whenever that water production stops. In the next step, the amount of 0.19 g Sb_2O_3 was added to the system and the temperature was increased to 548 K, and a vacuum was applied to help EG removal and polycondensation progress. The synthesized PET was removed from the reactor after 2 h. The mixing rate was constant at 100 rpm over the whole process. Polymer weight in each batch was about 550 g.

Characterization of polymer

The intrinsic viscosity (IV) of samples was measured using solution viscometry based on ISO-1628-5 standard using a Lauda-Konigshofen viscometer at 298 ± 0.1 K. To do so, the solution of polymer in the dichloroacetic acid with 10 mg/mL concentration was prepared through agitating at 373 K. The acid end groups of samples were determined by gravimetric methodology. A solution containing 1 g of PET in a 70:30 mixture of *ortho*-cresol/chloroform was prepared under heating and reflux. The mixture was titrated with 0.5 M KOH solution in ethanol using a model 798 MPT Titrino Metrohm titrator with a Solvotrode model electrode. The potentiometry and Tiamo 2.4 software were used to determine the titration end. Acid number (AN) is the concentration of acidic group at the end of esterification.

The DEG content of samples was determined using a GC3800 model of Varian Co., gas chromatography. Hence, 1–1.5 g of sample in 30 mL methanol was prepared at 493 K for 2 h. Consequently, the mixture was cooled down, and dimethyl terephthalate crystals were separated using filtration. A BYK spectrophotometer was applied to measure L and b parameters as color indices. The amount of 5–10 mg PET with KBr was mixed to form a pellet for FTIR spectroscopy. FTIR spectra were produced using a Bruker FTIR spectrometer. Sample solution in trifluoroacetic

acid, including CDCl_3 , the detector locking, was prepared to obtain an ^1H NMR spectrum using a Bruker 400 MHz Ultra Shield branded instrument. A Swiss-made Mettler Toledo, 822e model instrument was applied to plot DSC curves. First, samples were heated and kept at 573 K for 3–5 min to eliminate their history. Accordingly, the samples were cooled as quickly as possible to obtain an amorphous polymer. Next, the sample was heated with a heating rate of 10 K/min to determine T_m . For non-isothermal tests, the sample was heated to 573 K, kept for 3–5 min and cooled at a cooling rate of Φ . After cooling down to the ambient temperature, the samples were heated again with a heating rate of 10 K/min to evaluate T_g , T_m , recrystallization and melting.

Results and discussion

PET samples were prepared based on the procedure that was explained in the experimental section. Also, the repeatability of the synthesis method was studied. The characterization of samples revealed that PET samples with the following features were produced: $\text{IV} = 0.5$, $\overline{M}_n = 9650$ Da, $\text{AN} = 30$ mg/KOHg at the end of the esterification step; $\text{AN} = 30$ mg/KOHg of the final sample; $\text{DEG} = 1.54\%$ (by weight), $L = 89.8$, $b = 6.8$, and melting point = 524.6 K. Number-average molecular weight was estimated based on the following equation [33]:

$$[\eta] = K \overline{M}_n^a = 67 \times 10^{-4} \overline{M}_n^{0.47} \quad (1)$$

Hence, polymer with suitable IV, molecular weight, and melting point was produced. The samples showed AN less than 35 mg KOH/g, DEG less than 3% (by weight), and COOH less than 25, indicating acceptable PET samples produced from a commercial point of view.

FTIR spectra

Figure 1 represents the FTIR spectra of the synthesized PET sample. All related peaks are presented, and their assignment is consistent with the literature [34]. Table 1 presents a list of observed peaks in the spectra [34]. fingerprint peaks are as follows: the peak at 1250 cm^{-1} for c–o–c asymmetric stretching/CCH asymmetric bending, the peak at 1720 cm^{-1} for C–C ring stretching/C=O stretching, the peak at 720 cm^{-1} for OCH symmetric bending and the peak at 3070 cm^{-1} for C–H aromatic stretching. Therefore, the presence of such bonds approved the production of PET.

^1H NMR analysis

Figure 2 depicts the ^1H NMR spectrum of the PET sample. The corresponding protons shifts are also illustrated in

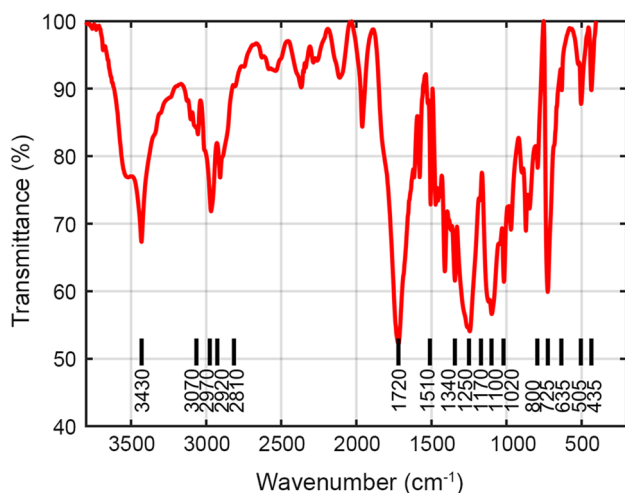


Fig. 1 FTIR spectra of prepared PET

Fig. 2, which are in agreement with the literature [35, 36]. Hence, PET was successfully synthesized, as it is consistent with the FTIR result.

Thermal behavior

Figure 3 illustrates the DSC plots of cooling curves with $\Phi = 5, 10, 15, 20, 30$ and 40 K/min cooling rates. These cooling rates were chosen according to the opinion of researchers reported in published articles. The data were plotted in three-dimensional coordinates to compare the crystallization trends. It is observed that the crystallization trend changes with changes in Φ . There is a bimodal trend for $\Phi = 15$ and

20 K/min. It is well known that PET presents primary and secondary crystallization. Dominance of primary or secondary crystallization depends on many parameters such as cooling rate. A bimodal peak is observed whenever both the primary and secondary regimes are comparably present [2, 3]. Hence, there is a change in the nature of crystallization form $\Phi = 5$ to 40 K/min. The overall degree of crystallinity during cooling is calculated by:

$$\chi_c = \frac{\Delta H_C}{\Delta H_{C_\infty}}, \quad (2)$$

where ΔH_C and $\Delta H_{C_\infty} = 84.52$ J/g are the measured heat of crystallization and complete crystallized PET, respectively [7]. The same calculation could be performed using melting enthalpy. The heat of fusion for crystallite PET is found to be $\Delta H_m^0 = 117.4$ J/g [37]. Table 2 presents the numerical values of different parameters. Figure 4 shows the DSC curves of the heating step. In Fig. 4, the peaks related to T_g , recrystallization and melting are detectable. Corresponding data are also presented in Table 2.

Analysis of data in Table 2 reveals valuable results. In Fig. 4 and Table 2, it can be found that there is a slight change in T_g . Therefore, the cooling rate and variation in the overall degree of crystallinity and quality of crystallites have no meaningful impact on the glass transition temperature. A typical DSC heating curve of partially crystallized PET shows the glass transition and melting temperatures as well as a recrystallization peak, at times called cold crystallization [4]. DSC heating curves for $\Phi = 5$ and 10 K/min show no recrystallization. It is deduced that at slow cooling rates such as $\Phi = 5$ and 10 K/min, crystallization is complete.

Table 1 FTIR characteristic peaks of PET sample

Location, cm^{-1}	Bond
3430	O–H stretching
3070	C–H asymmetric stretching/C–H aromatic stretching
2970	C–H symmetric stretching
2920	CH_2 asymmetric stretching
2810	CH_2 symmetric stretching
1720	C–C ring stretching/C=O stretching
1510	CH_2 scissoring
1340	CH_2 wagging
1250	CCH asymmetric bending/C–O–C asymmetric stretching
1170	C–O–C symmetric stretching/ CH_2 twisting/CCH symmetric bending
1100	C–O stretching
1020	C–C stretching
800	OCH asymmetric bending
725	OCH symmetric bending
635	CH_2 rocking
505	C–C bending/CCO asymmetric bending
435	C–O–C deformation/CCO symmetric bending

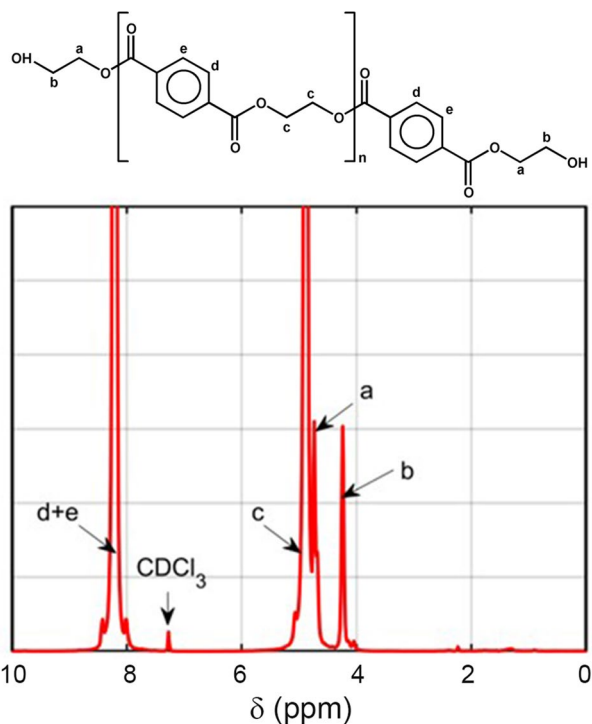


Fig. 2 ¹H NMR spectrum of PET sample

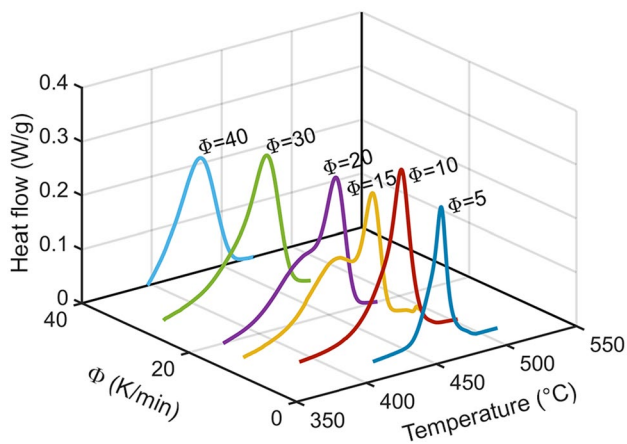


Fig. 3 DSC curves of sample cooling at different cooling rates

Table 2 DSC data results at various cooling rates*

Φ	T_C	ΔT_C	ΔH_C	χ_C	T_g	T_{Re}	ΔH_{Re}	T_m	ΔT_m	ΔH_m	χ_m	$t_{1/2}$	$T_{1/2}$
5	199.41	18.31	45.35	54	80.60	–	–	249.79	17.78	44.61	38	8.42	197.79
10	190.15	28.11	42.58	50	79.40	–	–	249.14	19.37	39.11	33	4.40	186.57
15	188.54	28.79	36.85	44	79.08	142.85	4.16	246.39	21.28	34.84	30	3.52	171.40
20	181.65	35.08	26.18	31	79.30	142.57	10.23	246.26	21.19	31.74	27	2.06	170.36
30	170.31	45.25	17.06	20	79.48	142.30	14.64	246.28	22.17	32.37	28	1.27	164.25
40	161.60	50.26	9.77	12	78.88	142.34	16.89	246.29	22.50	33.13	28	1.03	158.95t

*Temperatures are in °C, enthalpies are in J/g and crystallinity percentages are in % and fixed

However, at higher cooling rates, partial crystallization happens. A higher cooling rate gives less crystallization. Therefore, in heating curves, a larger recrystallization peak is observed. Nevertheless, the location of recrystallization peaks remains unchanged. The same is valid for melting temperature. For samples without recrystallization, the melting point is around 522 K, while it is around 519 K for samples with recrystallization. Although the difference is not much, it can be attributed to the quality and quantity of crystals. Small dependency of T_m was also reported previously [1]. DSC curves of $\Phi = 5$ and 10 K/min present a small shoulder in the beginning of melting peaks. Such a shoulder was reported previously and contributed to the existence of microcrystallite that is formed in the boundary layer between the larger crystallites [11]. Even the presence of three melting points was also reported [38]. Thermal history is one of the most important reasons for such observation. It is observed that T_C and χ_C are strongly a function of Φ . Figure 5 presents T_C and χ_C versus Φ . It is interesting that both T_C and χ_C change linearly. Also, in the literature, it was reported that crystallization exotherms shift to lower temperatures with increase in Φ [2, 7], which can be explained by the dynamic nature of crystallization. Crystallization consists of nucleation and growth steps. At higher cooling rates, longer time is required for sufficient nucleation, which means lower temperatures. A linear function was fitted on each data with an acceptable regression coefficient.

Crystallization kinetics modeling

To study the crystallization kinetics, it is necessary to obtain a degree of crystallinity. DSC data were used to calculate the degree of crystallinity, χ_t , with respect to time, by integrating the areas under exothermic peaks:

$$\chi_t = \int_0^t \frac{dH_t}{dt} dt \bigg/ \int_0^\infty \frac{dH_t}{dt} dt, \tag{3}$$

where dH_t/dt , t and χ_t are heat flow, time, and degree of crystallinity, respectively. In the following, various models are introduced to calculate the degree of crystallinity:

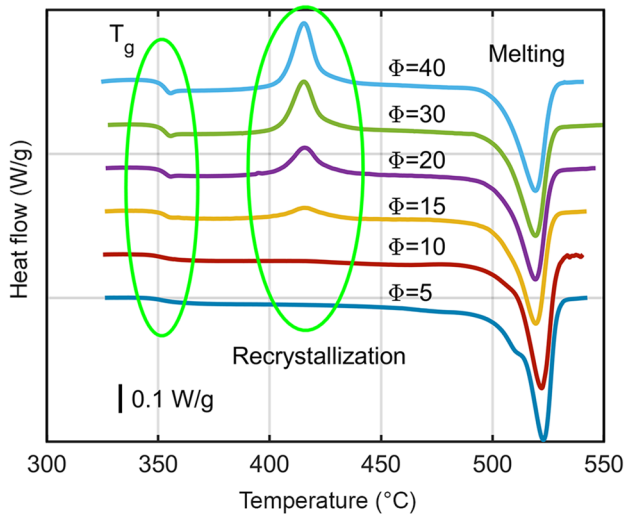


Fig. 4 DSC heating curve of PET samples

Modified Avrami model

The modified Avrami model is the basis for the most presented models. The Avrami model has been the most discussed model, giving the degree of crystallinity with respect to time:

$$\chi_t = 1 - \exp(-k \cdot t^n), \tag{4}$$

where k is the kinetic constant (a function of nucleation and growth rate), and n is the Avrami exponent (indicating nucleation mechanism). The main assumptions in this model are as follows: complete crystallization of samples, no change in volume throughout the process, constant growth rate and no secondary crystallization [28]. Initially, Avrami suggested this model for isothermal crystallization; then, it was modified and extended to non-isothermal models. In the latter case, the parameters concept would not be the same. It is well known that there is an incomplete crystallization, as given in Table 2 and shown in Fig. 5; Wunderlich introduced the final degree of crystallinity, χ_∞ , into the model to calculate relative crystallinity, $\chi_t[\chi_\infty]$:

$$\chi = \frac{\chi_t}{\chi_\infty} = 1 - \exp(-k \cdot t^n). \tag{5}$$

To acquire the model parameters, experimental data were fitted on the double logarithmic form:

$$\log(-\ln(1 - \chi)) = \log k + n \cdot \log t \quad k = \frac{0.69}{t_{1/2}^n}. \tag{6}$$

In this linear form, regression is a trivial task. Figure 6 depicts the comparison of the Avrami model and experimental data in the double logarithmic form.

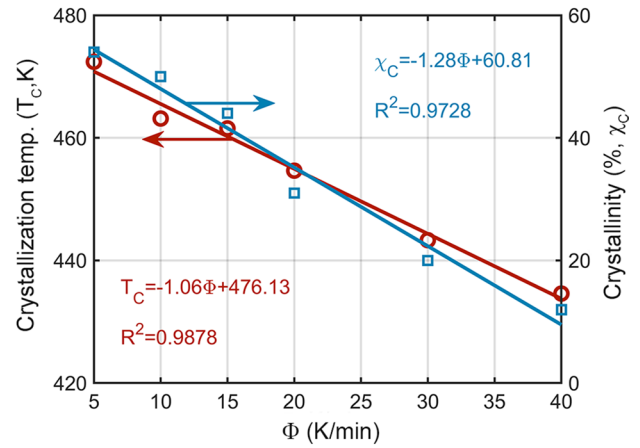


Fig. 5 Crystallinity temperature and percent versus cooling rate

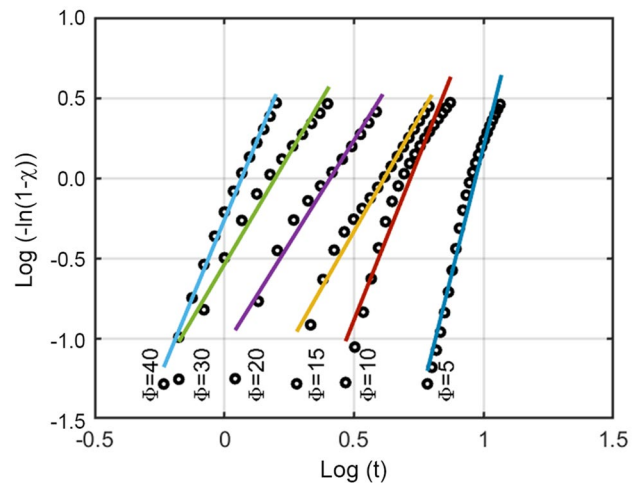


Fig. 6 Avrami model fitting results for relative crystallinity

The calculated model parameters, including regression coefficient (R^2), are given in Table 3. The Avrami exponent, n , value has a wide range. The range of 2.5–6.5 suggests that thermal nucleation occurs in the primary crystallization step, producing a three-dimensional spherical structure growth. Most of the crystallization happens in this step. A higher value of n means more three-dimensional structures than two-dimensional structures [2]. The extensive change in n is a sign of the asymmetry in crystallization behavior; therefore, different rate parameters would be calculated that are not comparable directly. The term k as the rate parameter indicates the overall crystallinity and its dependency on the process conditions. For example, k could be applied to determine the temperature of the maximum crystallization rate and the amount of crystal produced. A higher value of k demonstrates a higher nucleation density and growth rate. There is an immense variation in the k values; and in such

Table 3 Calculated model parameters

Avrami model						
Φ , °C/min	5	10	15	20	30	40
n	6.4615	4.9739	2.8333	2.5863	2.7469	3.9310
$\log k$	- 6.2630	- 2.9205	- 1.7489	- 1.0572	- 0.5390	- 0.2609
k	5.458×10^{-7}	0.0012	0.0178	0.0877	0.2891	0.5484
$k^{1/n}$	0.1073	0.2587	0.2414	0.3901	0.6365	0.8583
R^2	0.9739	0.9488	0.9703	0.9679	0.9711	0.9932
Ozawa model-primary stage						
T	160	170	180	190	200	
m	1.0527	2.8067	4.5579	6.2868	7.6135	
$\log K$	1.4416	3.7653	5.6875	7.1514	7.4502	
K	27.6419	5825.3	4.8698×10^5	1.4169×10^7	2.8200×10^7	
$K^{1/m}$	23.4092	21.9565	17.6944	13.7249	9.5182	
Ozawa model-secondary stage						
T	160	170	180	190	200	
m	1.0527	1.2090	1.4621	1.8812	2.7242	
$\log K$	1.4416	1.4768	1.5204	1.5352	1.5489	
K	27.6419	29.9765	33.1442	34.2909	35.3917	
$K^{1/m}$	23.4092	16.6546	10.9626	6.5475	3.7031	
Tobin model						
Φ	5	10	15	20	30	40
n_T	9.2903	6.0813	4.2496	3.8823	4.1111	5.5721
$\log K_T$	- 0.9300	- 0.6585	- 0.5386	- 0.3227	- 0.1111	- 0.0057
K_T	0.1175	0.2195	0.2894	0.4757	0.7743	0.9870
$(K_T)^{1/n_T}$	0.6809	0.7618	0.8005	0.8752	0.9551	0.9977
R^2	0.9908	0.9371	0.9841	0.9995	0.9915	0.9560
Hay model						
Φ	5	10	15	20	30	40
x_p	0.0502	2.675×10^{-5}	4.490×10^{-6}	2.464×10^{-6}	1.065×10^{-6}	1.142×10^{-6}
k_s	5.2062	13,058	86,108	192,649	566,914	657,819
n	7.8884	5.4710	2.5560	2.7109	3.3968	3.9689
k	5.04×10^{-8}	3.202×10^{-4}	4.627×10^{-2}	1.840×10^{-1}	5.985×10^{-1}	9.397×10^{-1}
$k^{1/n}$	0.1188	0.2297	0.3005	0.5355	0.8597	0.9845
R^2	0.99996	0.99999	0.99999	0.99999	0.99999	0.99999
Nakamura model						
Φ	5	10	15	20	30	40
n	2.7266	2.2508	2.0816	1.789	1.9088	2.0289
$(t_{1/2})_0$	4.1713	2.7463	2.7085	1.5238	0.9640	0.7963
U/R	0.9322	0.51161	0.24143	0.20097	0.1489	0.15609
T_∞	410.8960	386.5002	438.7171	409.0489	399.2570	406.6877
K_g	0.0001495	0.00015943	0.0001298	0.0001437	0.0001240	0.00007741
	0.0395	0.0206	0.0136	0.0071	0.0090	0.0094
R^2	0.99999	0.99999	0.99999	0.99999	0.99999	0.99999

a case, the normalized cooling rate, $k^{1/n}$, may be calculated with a unit of inverse time, namely the Avrami reduced rate constant. In the course of non-isothermal DSC, there are variations in nucleation and rate with respect to temperature. These variations could be taken into account by calculation of $k^{1/n}$ [40]. $k^{1/n}$ values are presented in Table 3. The variations in $k^{1/n}$ and n indicate a heterogeneous nucleation, leading to three-dimensional crystal growth. The R^2 values of models reveal an acceptable fitness for the relative crystallinity in the range of 10–90%. However, the inspection of the curves shows that there is a roll-off of around 60% relative crystallinity. This roll-off is contributed to the secondary crystallization that causes the deviation from the Avrami plots, as seen in Fig. 6. Therefore, the Avrami model is not a good predictor for crystallization kinetics. It is obvious that there is a change in the slope of the curve, indicating the existence of a secondary crystallization in PET.

Ozawa model

Ozawa introduced an equation for non-isothermal kinetics based on the kinetic analysis of thermo-analytical data of the process [41]. The primary assumption in this theory is that non-isothermal crystallization is an outcome of many small isothermal crystallization steps. This equation relates the cooling rate with time and temperature:

$$\chi = 1 - \exp\left(\frac{-K(T)}{\Phi^m}\right) \Rightarrow \log(-\ln(1-\chi)) = \log(K(T)) - m \log \Phi, \quad (7)$$

where m is the Ozawa exponent, and $K(T)$ is a cooling function at temperature T . For PET, in a small temperature range, parameter m , the Ozawa's exponent, is more or less constant [41]. However, in an extensive range, it varies with temperature. The Ozawa's exponent depends on the nucleation and crystalline growth geometry. Figure 7 illustrates the result of curve-fitting on Ozawa model and the resulting model parameters. It was expected that $\log(-\ln(1-\chi))$ would be linear versus $\log \Phi$; however, two distinct regimes are recognized, due to the primary and secondary crystallizations. These regions are determined in Fig. 7a; at a low relative crystallinity, when the primary process is dominant, while the secondary process is dominant at a high relative crystallinity. Moreover, the relative crystallinity corresponding to the change in crystallization regime decreases with the temperature increase. Due to these variations, the Ozawa analysis is limited, and this deviation is related to the primary and secondary crystallizations [42]. The calculated parameters of the Ozawa model at various cooling rates are given

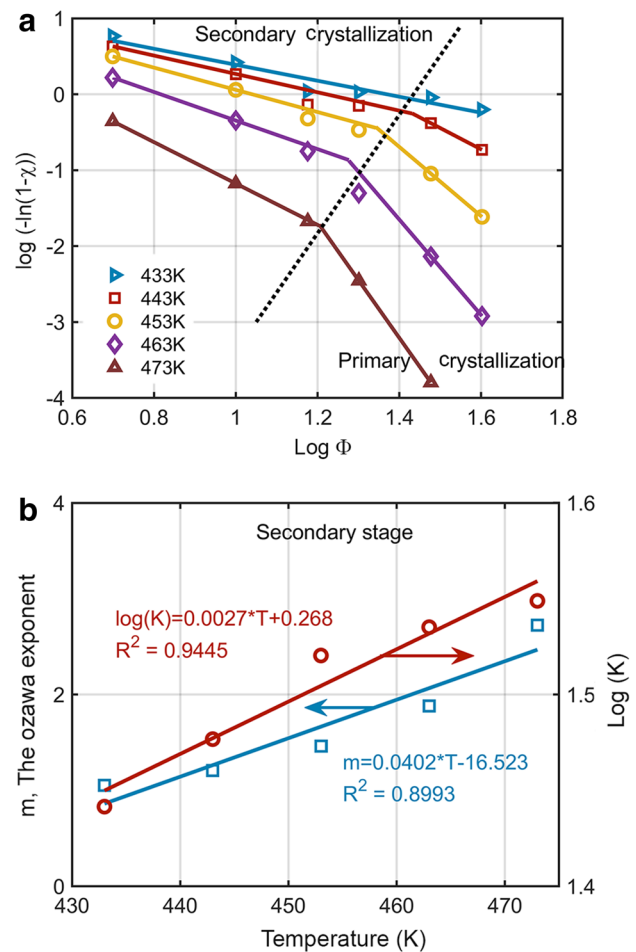


Fig. 7 Ozawa model fitting results: **a** double logarithmic of the Ozawa model plot and fitted lines, and **b** Ozawa model parameters versus temperature at the secondary stage

in Table 3. These parameters are presented in the primary as well as secondary crystallization stages. For the sake of comparison, the relative crystallinity at various cooling rates was calculated and plotted in Fig. 8. Based on the obtained data, the Ozawa model is not suitable for calculating the experimental relative crystallinity. The parameters evaluated in the secondary stage were applied in plotting Fig. 8. The results with the primary stage parameters are worse. Such a plot has not been observed in the literature, and the Ozawa model is not successful in modeling of non-isothermal crystallinity over a wide range of temperatures and cooling rates. It should be mentioned that in such a wide range of cooling rates, $\Phi \in [5, 40]$, the model error is very high, but the result is acceptable in a small range [34]. Nevertheless, the Ozawa's exponent, m , increases with temperature, and m is higher in the primary crystallization.

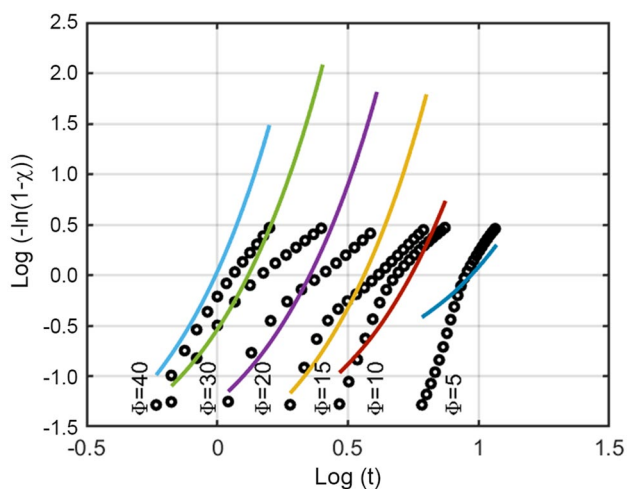


Fig. 8 Double logarithmic degree of crystallinity based on the Ozawa model

Tobin model

Taking into consideration secondary crystallization and impingement of spherulites, Tobin suggested the following model [43–45]:

$$\chi(t) = \frac{(K_T \cdot t)^{n_T}}{1 + (K_T \cdot t)^{n_T}} \Rightarrow \log\left(\frac{\chi(t)}{1 - \chi(t)}\right) = n_T \log K_T + n_T \log t, \tag{8}$$

where n_T is the Tobin's exponent and K_T is the Tobin's kinetic parameter. These parameters could be determined by plotting the logarithmic form, as given in Eq. 8. Table 3 reports the calculated parameters of the Tobin model at various cooling rates. The reduced rate constants for this model are also given. The Tobin's exponent is normally greater than the Avrami's exponent [46]. With simple mechanism for nucleation and growth, n_T is 2 and 3 for two- and three-dimensional networks [45]. Higher n_T could be contributed to the secondary crystallization of samples. Figure 9 shows the double logarithmic form of relative crystallinity obtained from the Tobin model. The model has the ability to show curvature in the plots.

So far, the main models that could be converted to linear form (double logarithmic equations) have been discussed. Hence, calculation of the model parameters would be an easy task. However, some models, which involve nonlinear regression, are introduced in the following, among which the Hay model is quite new.

Hay model

Recently, Hay et al. [27] have performed detailed studies on the primary and secondary crystallization of PET. They used

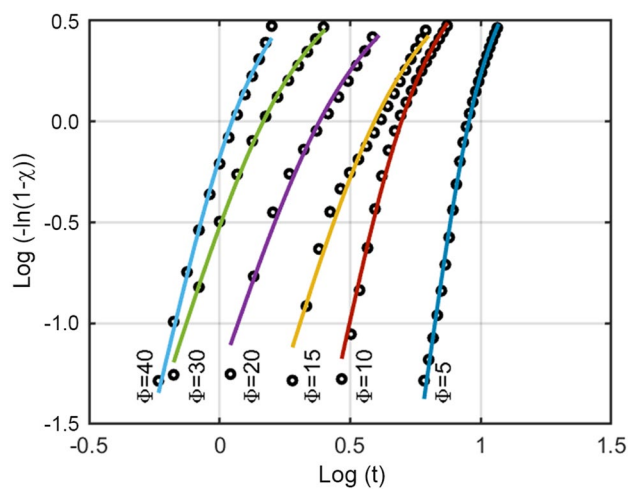


Fig. 9 Double logarithmic degree of crystallinity based on the Tobin model

DSC and FTIR methods to analyze the mechanism of crystallization. They observed a narrowing of the melting peak with heating after the primary crystallization and concluded that lamellae thickening happens in the secondary crystallization [47]. Furthermore, they studied the crystallization of PET using FTIR spectroscopy [48]. In general, they made a conclusion that in the course of the secondary crystallization, the local diffusion of chain segments increases the thickness of lamellae. They proposed that the secondary relative crystallinity rises proportionally to the square root of the crystallization time. In other words, secondary crystallization happens around the boundaries of the spherulites. Consequently, the total relative crystallization is the addition of primary and secondary processes. Hence, they suggested the following equation:

$$\chi = x_p(1 - \exp(-kt^n)) \cdot (1 + k_s \sqrt{t}), \tag{9}$$

where x_p is the degree of primary crystallinity, n is the Avrami's exponent for primary crystallization, k is the rate constant for nucleation and growth, and k_s is the rate constant for growth of the secondary crystallization. The comparison of Eqs. 5 and 9 demonstrates that the overall relative crystallization is a sum of two terms; the first one is described by the Avrami type equation related to the primary crystallization; the second term describes the secondary crystallization, which is a square root of time-weight of the first term. Assuming the same justification for the modified Avrami model, the Hay model was fitted to the non-isothermal data. Parameter calculation for the Hay model needs the use of nonlinear regression algorithms. The simplex method of

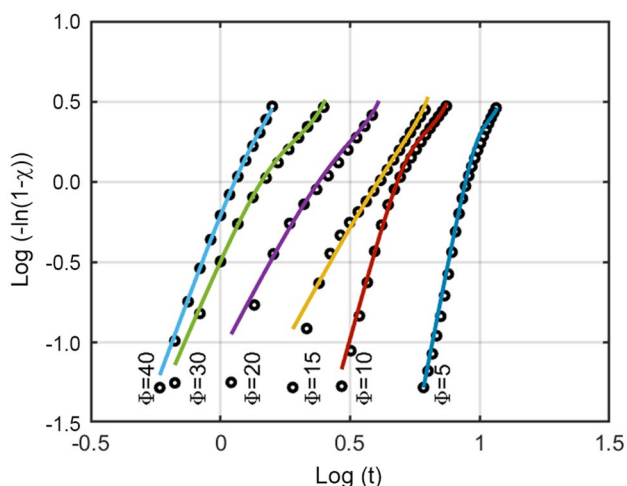


Fig. 10 Double logarithmic degree of crystallinity based on the Hay model

Lagarias et al. [49] was used by applying the least-square criterion that was employed as an objective function to calculate the model parameters:

$$\text{Objective function} = \sum_{i=1}^n (\chi_{\text{exp}} - \chi_{\text{model}})^2. \quad (10)$$

Due to the nonlinear nature of optimization, convergence problems are encountered. The convergence rate is very slow. Therefore, various objective functions were examined; the following is the best one:

$$\text{Objective function} = 1 - R^2, \quad (11)$$

where R^2 is the regression coefficient. Unfortunately, this objective function leads to another optimum point that is the normal nature of nonlinear problems; thus, a new algorithm was introduced. Calculation loop starts with Eq. 10 as an objective function, and whenever the regression coefficient reaches over 0.96, the objective function switches to Eq. 11. This approach suggested that the algorithm was successful in all calculations. Figure 10 presents the comparison of the experimental and the Hay model data. As can be observed, the Hay model has an excellent ability to predict the relative crystallinity compared to the Avrami model. The only slight deviations observed at cooling rates $\Phi = 15$ and 20 K/min could be attributed to the bimodal nature of the degree of crystallization, as seen in the Fig. 3. Despite the variation in

parameters, the reduced rate constant gives a smooth trend in model interpretation.

Nakamura model

Nakamura model was suggested and applied for non-isothermal crystallization [50–52]. This model assumes that non-isothermal crystallization is a series of many small isothermal steps. Consequently, each step could be described by the Avrami model. Nakamura et al. presented the following equation:

$$\chi(t) = 1 - \exp\left(-\int_0^t k(T) dt\right)^n. \quad (12)$$

Typically, to acquire the Nakamura model parameters, the differential form of Eq. 12 was applied:

$$\frac{d\chi}{dt} = n \cdot k(T)(1 - \chi) [-\ln(1 - \chi)]^{\frac{n-1}{n}}. \quad (13)$$

However, the differentiation of experimental data intensifies random errors during real time data gathering. Therefore, in this work, it is suggested to use the original integral form of Equation 13:

$$\chi = \int_0^{\chi} d\chi = \int_0^t n \cdot k(T)(1 - \chi) [-\ln(1 - \chi)]^{\frac{n-1}{n}} dt. \quad (14)$$

To do so, nonlinear regression was applied. The expression $k(T)$ was needed to be able to continue calculations. Hoffman-Lauritzen suggested the following equation for the secondary nucleation theory [53]:

$$k(T) = \frac{(\ln 2)^{\frac{1}{n}}}{(t_{1/2})_0} \exp\left(\frac{-U/R}{T - T_{\infty}}\right) \exp\left(\frac{-K_g}{T\Delta T f}\right) \text{ where } \Delta T = T_m^0 - T \quad \& \quad f = \frac{2T}{T_m^0 + T}, \quad (15)$$

where: U is the crystalline molecular transport activation energy between crystal and melt; $(t_{1/2})_0$ is a factor including all temperature-independent terms; K_g is the secondary nucleation constant; T_{∞} is a hypothetical temperature that molecular transport starts; T_m^0 is the equilibrium melting temperature, ΔT is the under-cooling degree; f is a correction factor to take into account the bulk enthalpy of fusion variation; and R is the universal gas constant. The crystallization time can be converted to crystallization temperature:

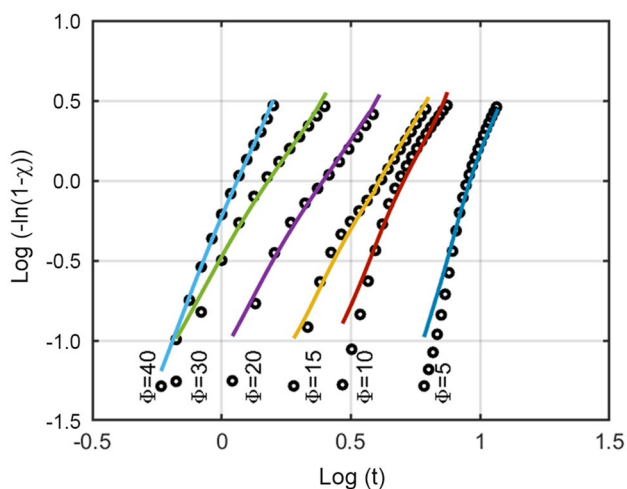


Fig. 11 Nakamura model results

$$t = \frac{T_0 - T}{\Phi} \Rightarrow dt = -\frac{dT}{\Phi} \tag{16}$$

The final equation is:

$$\chi = \int_0^t n \cdot \frac{(\ln 2)^{\frac{1}{n}}}{(t_{1/2})_0} \exp\left(\frac{-U/R}{T - T_\infty}\right) \exp\left(\frac{-(T_m^0 + T)K_g}{2T^2(T_m^0 - T)}\right) (1 - \chi) [-\ln(1 - \chi)]^{\frac{n-1}{n}} \frac{-dT}{\Phi} \tag{17}$$

Due to its highly nonlinear nature, initial postulates for parameters are very important in the fitting calculation. Hence, 3 for the Avrami's exponent and T_g-30 for T_∞ were selected. The optimization of fitting parameters was performed using the simplex method of Lagarias et al. [49]. Hoffman and Weeks theory was applied to assess the correct equilibrium temperature [54]:

$$T_m = T_m^0 \left(1 - \frac{1}{\beta}\right) + \frac{T_C}{\beta} \tag{18}$$

where factor β depends on the final thickness of lamellar. Using the data in Table 3, T_m^0 and β were estimated to be 504.28 K and 11.31, respectively. The experimental estimation of U is a difficult task. However, using DSC data, it is possible to predict such parameters. Similar to the calculation algorithm for the Hay model, the objective function was changed during the calculation to obtain the appropriate regression coefficient. Table 3 gives the calculated Hoffman-Lauritzen parameters. Figure 11 shows the comparison of the experimental and Nakamura model results.

In Fig. 11, it can be seen that the Lauritzen-Hoffman model clearly could point out the presence of secondary crystallization. However, at the beginning of crystallization, in which

the primary process is dominant, this model is less successful than the end of the process with the dominant secondary crystallization.

Conclusion

Due to dependency of the final properties of polymeric parts, it is vital to have information about non-isothermal crystallization from melt state. Although, many research results have been published in the crystallization behavior of PET, still there are more information to be studied. Hence, additive free polyethylene terephthalate was synthesized through direct esterification of TPA and EG, and then polycondensation at 513 and 548 K, respectively. Fingerprint peaks of PET were recognized in the FTIR spectrum. ¹H NMR spectrum of PET was consistent with its chemical structure. Therefore, suitable PET samples were prepared. Moreover, their determined properties showed that very fine PET samples were at hand. Consequently, the non-isothermal crystallization behavior of samples was studied. Non-isothermal crystallization studies were per-

formed in a wide range of cooling rates, namely 5, 10, 15, 20, 30 and 40 K/min. This range is comparable to the cooling rate during the production of PET products. Although, the modified Avrami is one of the most widely used models, it is seen that it cannot take into account the secondary crystallization. A change in slope and deviation from linear behavior in the double logarithmic plot is an indication of a secondary crystallization. Tobin's model has the ability to fit experimental data. However, Hay and Nakamura models have better physical background.

The newly introduced Hay model has an excellent ability to describe the crystallization kinetics. Nakamura model associated with Hoffman-Lauritzen expression, with a theoretical background, fitted the data well. The results demonstrated that the Hay model is the most suitable model for the non-isothermal crystallization kinetics of polyethylene terephthalate from the melt state.

Funding No funding was given to this research.

Declarations

Conflict of interest The authors declare that they do not have any conflict of interest.

References

- Hafsia KB, Ponçot M, Chapron D, Royaud I, Dahoun A, Bourson P (2016) A novel approach to study the isothermal and non-isothermal crystallization kinetics of poly (ethylene terephthalate) by Raman spectroscopy. *J Polym Res* 23:1–14
- Gaonkar AA, Murudkar VV, Deshpande VD (2020) Comparison of crystallization kinetics of polyethylene terephthalate (PET) and reorganized PET. *Thermochim Acta* 683:178472
- Heidrich D, Gehde M (2022) The 3-phase structure of polyesters (PBT, PET) after isothermal and non-isothermal crystallization. *Polymers* 14:793
- Jog JP (1995) Crystallization of polyethylene terephthalate. *J Macromol Sci C* 35:531–553
- Van Antwerpen F, Van Krevelen DW (1972) Influence of crystallization temperature, molecular weight, and additives on the crystallization kinetics of poly (ethylene terephthalate). *J Polym Sci B* 10:2423–2435
- Jabarin SA (1987) Crystallization kinetics of polyethylene terephthalate: I) isothermal crystallization from the melt. *J Appl Polym Sci* 34:85–96
- Jabarin SA (1987) Crystallization kinetics of polyethylene terephthalate: II) dynamic crystallization of PET. *J Appl Polym Sci* 34:97–102
- Phillips PJ, Tseng HT (1989) Influence of pressure on crystallization in poly (ethylene terephthalate). *Macromolecules* 22:1649–1655
- Jiang XL, Luo SJ, Sun K, Chen XD (2007) Effect of nucleating agents on crystallization kinetics of PET. *Express Polym Lett* 1:245–251
- Deetum C, Samthong C, Choksrivichit S, Somwangthanoj A (2020) Isothermal cold crystallization kinetics and properties of thermoformed poly (lactic acid) composites: effects of talc, calcium carbonate, cassava starch and silane coupling agents. *Iran Polym J* 29:103–116
- Wang G, Chen Y (2018) Isothermal crystallization and spherulite morphology of poly (ethylene terephthalate)/Na⁺-MMT nanocomposites prepared through solid-state mechanochemical method. *J Therm Anal Calorim* 131:2611–2624
- Thamizhlarasan A, Meenarathi B, Parthasarathy V, Jancirani A, Anbarasan R (2021) Effect of nucleating agents on the non-isothermal crystallization and degradation kinetics of poly (ethylene terephthalate). *Polym Adv Technol* 32:766–778
- Sohrabi A, Rafizadeh M (2022) Non-isothermal crystallization and thermo-mechanical properties of poly (butylene adipate-co-ethylene terephthalate) random copolyesters. *Thermochim Acta* 2:179252
- Mohammadi Avarzman A, Rafizadeh M, Afshar Taromi F (2021) Branched polyester based on the polyethylene terephthalate and trimellitic anhydride as branching agent. *Polym Bull* 79:6099–6121
- Kahkesh S, Rafizadeh M (2020) Flame retardancy and thermal properties of poly (butylene succinate)/nano-boehmite composites prepared via in situ polymerization. *Polym Eng Sci* 60:2262–2271
- Topkanlo HA, Ahmadi Z, Taromi FA (2018) An in-depth study on crystallization kinetics of PET/PLA blends. *Iran Polym J* 27:13–22
- Groeninckx G, Berghmans H, Overbergh N, Smets G (1974) Crystallization of poly (ethylene terephthalate) induced by inorganic compounds: I) crystallization behavior from the glassy state in a low-temperature region. *J Polym Sci B* 12:303–316
- Johnson JE (1959) X-ray diffraction studies of the crystallinity in polyethylene terephthalate. *J Appl Polym Sci* 2:205–209
- Fielding-Russell GS, Pillai PS (1970) A study of the crystallization of polyethylene terephthalate using differential scanning calorimetry and X-ray techniques. *Die Makromol Chem* 135:263–274
- Elsner G, Koch MHJ, Bordas J, Zachmann HG (1981) Time resolved small angle scattering during isothermal crystallization of unoriented poly (ethylene terephthalate) using synchrotron radiation. *Die Makromol Chem* 182:1263–1269
- Engelbrecht S, Tybussek KH, Sampaio J, Böhmeler J, Fischer BM, Sommer S (2019) Monitoring the isothermal crystallization kinetics of PET-A using THz-TDS. *J Infrared Millim Terahertz Waves* 40:306–313
- Menczel JD, Prime RB (2009) *Thermal analysis of polymers: fundamentals and applications*. Wiley, New Jersey
- Mohammadi S, Taremi FA, Rafizadeh M (2012) Crystallization conditions effect on molecular weight of solid-state polymerized poly (ethylene terephthalate). *Iran Polym J* 21:415–422
- Lemanowicz M, Mielańczyk A, Walica T, Kotek M, Gierczycki A (2021) Application of polymers as a tool in crystallization: a review. *Polymers* 13:2695
- Wang ZG, Hsiao BS, Sauer BB, Kampert WG (1999) The nature of secondary crystallization in poly (ethylene terephthalate). *Polymer* 40:4615–4627
- Lu XF, Hay JN (2001) Isothermal crystallization kinetics and melting behaviour of poly (ethylene terephthalate). *Polymer* 42:9423–9431
- Chen Z, Hay JN, Jenkins MJ (2016) The effect of secondary crystallization on crystallization kinetics—polyethylene terephthalate revisited. *Eur Polym J* 81:216–223
- Verhoyen O, Dupret F, Legras R (1998) Isothermal and non-isothermal crystallization kinetics of polyethylene terephthalate: mathematical modeling and experimental measurement. *Polym Eng Sci* 38:1594–1610
- Balamurugan GP, Maiti SN (2008) Nonisothermal crystallization kinetics of polyamide 6 and ethylene-co-butyl acrylate blends. *J Appl Polym Sci* 107:2414–2435
- Meng C, Liu X (2022) Isothermal crystallization kinetics of bio-based semi-aromatic high-temperature polyamide PA5T/56. *Iran Polym J* 31:605–617
- Yao H, Li W, Zeng Z, Wang T, Zhu J, Lin Z (2022) Non-isothermal crystallization kinetics of poly (phthalazinone ether sulfone)/MC nylon 6 in-situ composites. *Iran Polym J* 31:869–882
- Mahalakshmi S, Kannammal L, Tung KL, Anbarasan R, Parthasarathy V, Alagesan T (2019) Evaluation of kinetic parameters for the crystallization and degradation process of synthesized strontium mercaptosuccinate functionalized poly (ϵ -caprolactone) by non-isothermal approach. *Iran Polym J* 28:549–562
- Sánchez-Arrieta N, De Ilarduya AM, Alla A, Muñoz-Guerra S (2005) Poly (ethylene terephthalate) copolymers containing 1, 4-cyclohexane dicarboxylate units. *Eur Polym J* 41:1493–1501
- Charles J, Ramkumaar GR (2009) FTIR and thermal studies on polyethylene terephthalate and acrylonitrile butadiene styrene. *Asian J Chem* 21:4389–4398
- Chang SJ, Chang FC (1999) Synthesis and characterization of copolyesters containing the phosphorus linking pendent groups. *J Appl Polym Sci* 72:109–122
- Han Z, Wang Y, Wang J, Wang S, Zhuang H, Liu J, Tang J (2018) Preparation of hybrid nanoparticle nucleating agents and their effects on the crystallization behavior of poly (ethylene terephthalate). *Materials* 11:587
- Smith CW, Dole M (1956) Specific heat of synthetic high polymers: VII) polyethylene terephthalate. *J Polym Sci* 20:37–56
- Phang IY, Pramoda KP, Liu T, He C (2004) Crystallization and melting behavior of polyester/clay nanocomposites. *Polym Int* 53:1282–1289

39. Lin CC (1983) The rate of crystallization of poly (ethylene terephthalate) by differential scanning calorimetry. *Polym Eng Sci* 23:113–116
40. Torrens-Serra J, Venkataraman S, Stoica M, Kuehn U, Roth S, Eckert J (2011) Non-isothermal kinetic analysis of the crystallization of metallic glasses using the master curve method. *Materials* 4:2231–2243
41. Ozawa T (1971) Kinetics of non-isothermal crystallization. *Polymer* 12:150–158
42. Heidarzadeh N, Rafizadeh M, Afshar Taromi F, Puiggali J, del Valle LJ (2019) Nucleating and retarding effects of nanohydroxyapatite on the crystallization of poly (butylene terephthalate-co-alkylenedicarboxylate)s with different lengths. *J Therm Anal Calorim* 137:421–435
43. Tobin MC (1974) Theory of phase transition kinetics with growth site impingement: I. homogeneous nucleation. *J Polym Sci B* 12:399–406
44. Tobin MC (1976) The theory of phase transition kinetics with growth site impingement. II Heterogeneous nucleation. *J Polym Sci B* 14:2253–2257
45. Tobin MC (1977) Theory of phase transition kinetics with growth site impingement: III) mixed heterogeneous-homogeneous nucleation and nonintegral exponent of the time. *J Polym Sci B* 15:2269–2270
46. Ravindranath K, Jog JP (1993) Polymer crystallization kinetics: poly (ethylene terephthalate) and poly (phenylene sulfide). *J Appl Polym Sci* 49:1395–1403
47. Chen Z, Jenkins MJ, Hay JN (2014) Annealing of poly (ethylene terephthalate). *Eur Polym J* 50:235–242
48. Chen Z, Hay JN, Jenkins MJ (2013) The effect of secondary crystallization on melting. *Eur Polym J* 49:2697–2703
49. Lagarias JC, Reeds JA, Wright MH, Wright PE (1998) Convergence properties of the Nelder-Mead simplex method in low dimensions. *SIAM J Optim* 9:112–147
50. Nakamura K, Watanabe T, Katayama K, Amano T (1972) Some aspects of nonisothermal crystallization of polymers: I. Relationship between crystallization temperature, crystallinity, and cooling conditions. *J Appl Polym Sci* 16:1077–1091
51. Nakamura K, Katayama K, Amano T (1973) Some aspects of nonisothermal crystallization of polymers: II. Consideration of the isokinetic condition. *J Appl Polym Sci* 17:1031–1041
52. Seo J, Zhang X, Schaake RP, Rhoades AM, Colby RH (2021) Dual Nakamura model for primary and secondary crystallization applied to nonisothermal crystallization of poly (ether ether ketone). *Polym Eng Sci* 61:2416–2426
53. Hoffman JD, Davis GT, Lauritzen JI (1976) In: Hannay NB (ed) *Treatise on solid state chemistry*. Springer, Boston
54. Marand H, Xu J, Srinivas S (1998) Determination of the equilibrium melting temperature of polymer crystals: linear and nonlinear Hoffman–Weeks extrapolations. *Macromolecules* 31:8219–8229

Springer Nature or its licensor (e.g. a society or other partner) holds exclusive rights to this article under a publishing agreement with the author(s) or other rightsholder(s); author self-archiving of the accepted manuscript version of this article is solely governed by the terms of such publishing agreement and applicable law.